

NASA REPORT DOCUMENTATION PAGE (IN LIEU OF NASA FORM SF 298)

1. REPORT NO.	2. GOVERNMENT ACCESSION NO.	3. RECIPIENT'S CATALOG NO.
4. TITLE AND SUBTITLE Signatures of Nonlinear Waves in Coronal Plumes and Holes		5. REPORT DATE CODE:
7. AUTHOR(S) Dr. Leon Ofman		8. PERFORMING ORGANIZA- TION REPORT NO:
9. PERFORMING ORGANIZATION NAME AND ADDRESS Raytheon ITSS Corporation 4400 Forbes Blvd. Lanham, MD 20706		10. WORK UNIT NO.
12. SPONSORING AGENCY NAME AND ADDRESS Goddard Space Flight Center Headquarters Procurement Office Code 210.H Greenbelt, MD 20771		11. CONTRACT OR GRANT NO. NASW-98024
		13. TYPE OF REPORT AND PERIOD COVERED Final progress report: September 21, 1998 - November 12, 1999
		14. SPONSORING AGENCY CODE NASA / CODE 210.H
15. SUPPLEMENTARY NOTES		
16. ABSTRACT In recent UVCS/SOHO White Light Channel (WLC) observations we found quasi-periodic variations in the polarized brightness (pB) in the polar coronal holes at heliocentric distances of 1.9-2.45 solar radii. The motivation for the observation is the 2.5D MHD model of solar wind acceleration by nonlinear waves, that predicts compressive fluctuations in coronal holes. To help identify the waves observed with the UVCS/WLC we model the propagation and dissipation of slow magnetosonic waves in polar plumes using 1D MHD code in spherical geometry. We find that the slow waves nonlinearly steepen in the gravitationally stratified plumes. The nonlinear steepening of the waves leads to enhanced dissipation due to compressive viscosity at the wave-fronts.		
17. KEY WORDS (SUGGESTED BY AUTHOR(S)) Solar Corona, Waves, Coronal Holes,		18. DISTRIBUTION STATEMENT Space Science, Solar Physics
19. SECURITY CLASSIF. None	20. SECURITY CLASSIF. None	21. NO OF PAGES   22. PRICE

# Signatures of Nonlinear Waves in Coronal Plumes and Holes

## Final Report for 9/21/98-11/12/99

### 1. Publications and Meetings Attended

Below is the list of publications, and meetings attended in the period covered by this report that were supported in full or in part by this program.

- Ofman, L., Romoli, M., Poletto, G., Noci G., Kohl, J.L., UVCS WLC Observations of Compressional Waves in the South Polar Coronal Hole, *The Astrophysical Journal*, 1999, in press.
- Ofman, L., Romoli, M., Noci, G., Poletto, G., Kohl, J.L., Howard, R.A., St. Cyr, C., SOHO Observations of Density Fluctuations in Coronal Holes, *Space Science Reviews*, 87, 165, 1999.
- Ofman, L., V. Nakariakov, C.E. DeForest, Slow Magnetosonic Waves in Coronal Plumes, *The Astrophysical Journal*, 514, 441, 1999.
- Ofman, L., V.M. Nakariakov, N. Sehgal, Dissipation of Slow Magnetosonic Waves in Coronal Plumes, *The Astrophysical Journal*, 1999, submitted.
- Ofman, L., and C.E. DeForest, Numerical Simulations of Trapped Sound Waves in Solar Coronal Plumes, 32nd COSPAR Scientific Assembly, *Advances in Space Research*, 1999, in press.
- Ofman, L., Propagation and Dissipation of Slow Magnetosonic Waves in Coronal Plumes, *The last total solar eclipse of the millennium in Turkey*, W. Livingston and A. Ozguc (eds.), *PASP*, 1999, submitted.
- Ofman, L., Davila, J.M., Two-fluid 2.5D MHD Model of the Fast Solar Wind and the Effective Proton Temperature, in *Solar Wind Nine*, S. Habbal et al. (eds), *AIP Conference Proceedings*, 471, pp. 405-408, AIP, New York, 1999.
- Davila, J.M., Ofman, L., Two-fluid 2.5D MHD Simulations of the Fast Solar Wind in Coronal Holes and the Relation to UVCS Observations, *Space Science Reviews*, 87, 287, 1999.
- V.M. Nakariakov, Ofman, L., T.D. Arber, Nonlinear Dissipative Spherical Alfvén Waves in Solar Coronal Holes, *Astronomy and Astrophysics*, 1999, in press.

**UVCS WLC Observations of Compressional Waves in the South  
Polar Coronal Hole**

L. Ofman

Raytheon ITSS and NASA Goddard Space Flight Center, Mail code 682, Greenbelt, MD  
20771, USA

M. Romoli

Department of Astronomy and Space Science, University of Florence, Largo Fermi 5, 50125  
Florence, Italy

G. Poletto

Arcetri Observatory, I-50125 Florence, Italy

G. Noci

Department of Astronomy and Space Science, University of Florence, Largo Fermi 5, 50125  
Florence, Italy

J.L. Kohl

Harvard-Smithsonian Center for Astrophysics, 60 Garden st, Cambridge, MA 02138, USA

Received \_\_\_\_\_; accepted \_\_\_\_\_

Astrophysical Journal, to appear January 20, 2000.

## ABSTRACT

Recent SOHO UVCS White Light Channel (WLC) observations of the south polar coronal hole plumes and interplume regions produce signatures of quasi-periodic variations in the polarized brightness (pB) at a heliocentric distance of 1.9 solar radii ( $R_{\odot}$ ). The Fourier power spectrum of the pB time series shows significant peaks at about 1.6-2.5 mHz and additional smaller peaks at longer and shorter time scales. Wavelet analysis of the pB time series shows that the coherence time of the fluctuations is about 30 minutes. The new observations strongly suggest that the fluctuations are compressional wave packets propagating in the coronal hole high above the limb. The presence of compressional waves may have important implications that help to explain the heating of coronal holes and the fast solar wind acceleration.

*Subject headings:* solar wind—Sun: corona—Sun: magnetic fields—waves—MHD

## 1. Introduction

The detection of density fluctuations in coronal holes is a difficult task due to the low coronal hole density ( $\sim 5 \times 10^7 \text{ cm}^{-3}$  at  $1.16R_{\odot}$ , Fisher & Guhathakurta 1995) and the corresponding low light emission of the coronal hole plasma. Recent high-cadence observations by Ofman et al. (1997) of coronal holes using the white light channel (WLC) of the Ultraviolet Coronagraph Spectrometer (UVCS) (Kohl et al. 1995) were the first to show polarized brightness (pB) fluctuations on a time scale of  $\sim 10$  min high above the limb at  $1.9R_{\odot}$ . Ofman et al. (1997, 1998) interpreted these quasi-periodic fluctuations as density fluctuations due to compressional waves propagating in the coronal hole. The Extreme Ultraviolet Telescope EIT (Delaboudinière et al. 1995) on board SOHO reports compressional slow waves in coronal hole plumes below  $1.2R_{\odot}$  (DeForest et al. 1997, DeForest and Gurman 1998, Ofman, Nakariakov & DeForest 1999). In particular, DeForest and Gurman (1998) observed quasiperiodic fluctuations in the brightness of Fe IX and Fe X line emissions at  $171\text{\AA}$  on a timescale of a few to ten minutes that coherently propagate outward at speeds of  $\sim 75\text{-}150 \text{ km s}^{-1}$ . Ofman, Nakariakov, & DeForest (1999) have identified these propagating fluctuations as slow magnetosonic waves. It is likely that the waves detected by Ofman et al. (1997) at  $1.9R_{\odot}$  are of the same nature as the waves detected by DeForest and Gurman (1998) lower in coronal holes.

The energy flux contained in the slow magnetosonic waves detected by DeForest and Gurman (1998) is not sufficient for coronal heating. However, only part of the wave flux may have been detected. The compressional waves may carry a significant fraction of the energy that is required to heat the coronal holes (Ofman, Nakariakov & DeForest 1999). The efficient dissipation of the slow waves by compressive viscosity close to the sun, and by Landau damping in the collisionless plasma suggest that the waves may contribute to heating of the coronal holes in the first solar radii above the limb. This region in coronal

holes is difficult to heat by shear Alfvén waves due to their large dissipation length, even when phase mixing is taken into account (Ofman & Davila 1995). The compressional waves may provide a signature of the nonlinear wave acceleration mechanism proposed by Ofman & Davila (1997a, 1997b, 1998) for the acceleration of the fast solar wind.

Below, we report the results of the new UVCS WLC observations of coronal hole density fluctuations with longer duration, and higher cadence. In § 2 we describe the method of observations at one and at two radial positions, together with the error analysis. In § 3 we show the observational results. We have applied the fast Fourier transform (FFT) and the wavelet analysis to our data. We performed the cross-correlation analysis at two radial positions in order to determine the propagation speed of the fluctuations. The conclusions are in § 4. The observations suggest that the pB fluctuations are due to propagating compressional wave packets in coronal holes.

## 2. Observational Method

### 2.1. Observations at one radial position

The observational method of the pB with the WLC is described in detail in Ofman et al. (1997). Here, we present a brief summary of the method. The WLC is a polarimeter that measures the pB in the 450-600 nm band, over a  $14 \times 14$  square arc-second area located at the center of the instantaneous UVCS field of view. The coronal pB can be directly related to the electron density integrated over the line of sight. Because the UVCS field of view can be rotated about the Sun center, the WLC can look at different position angles. The WLC measurements and the most recent calibration are described in Romoli et al (1997).

The purpose of the measurements reported below is to investigate low frequency

(milli-Hertz) electron density fluctuations. The determination of the absolute magnitude of the electron density is left for future studies. The instrumental polarized stray light, which is usually removed from the pB measurement, constitutes a constant and negligible contribution to the total pB at the heights of interest. The time resolution is constrained by the required signal to noise ratio of the pB intensity. The noise in the pB intensity is determined by photon statistics. The number of photons that reach the detector decreases with the heliocentric height of the pB measurement. In order to improve the time resolution, we assume that the pB polarization plane is tangent to the solar limb. This allows us to reduce the number of polarizer positions from three to two to obtain a pB measurement. The pB counts are obtained by taking the difference in counts between two successive positions of the polarizer.

The line-of-sight averaging of the white light data probably reduces the variation of the pB due to the compressional waves. This effect must be taken into account when determining the amplitude of the waves from the observations in future studies. Looking at plumes may reduce the dilution due to line-of-sight integration, since the waves may propagate in phase due to trapping (Ofman, Nakariakov & DeForest 1999), minimizing line of sight integration effects on the signal. When interplume regions are considered only the largest amplitude fluctuations in the line of sight (i.e., localized density enhancements) will contribute to the pB intensity, minimizing the line-of-sight dilution.

## 2.2. Observations at two radial positions

In order to determine the phase speed of the density fluctuations we performed time resolved observations with the WLC pointing at two radial distances from the Sun with a cadence of about 5 minutes. This method is based on the finite propagation velocity of the waves carried by the solar wind. By alternating the observation of the pB between  $1.9 R_{\odot}$

and  $2.1 R_{\odot}$  at a rate shorter than the expected travel time of the disturbances between the two points (on the same magnetic structure) it may be possible to observe a correlation between the pB fluctuations at the two points. This correlation will allow measurement of the propagation speed of the disturbances by calculating the travel time that yields the best correlation between the two time series. If the solar wind speed is independently known, then this travel time can be used to determine the phase speed of the waves, which then will be compared to the model predictions.

In particular, we have used the following technique to measure the phase speed of the waves. The UVCS was pointed above one of the poles, and the WLC was observing along the radial direction at an area of  $14 \times 14$  arc-seconds. The maximum time assigned to continuous observation was several hours (see Table 1). During the observing run, we obtained three pB measurements at  $1.9R_{\odot}$  followed by three pB measurements at  $2.1R_{\odot}$ . This sequence was repeated for the duration of the observation. We assumed that the angle of polarization did not change so that two positions of the polarizer are sufficient to derive the pB. As discussed below, 30-60 second exposures for each polarizer position are enough to achieve accuracy better than 10% on the pB measurement. The cadence was determined by the combination of the exposure time and the instrument mirror pointing time.

### 2.3. Error analysis

In order to estimate the signal-to-noise ratio (S/N) in our observation we define  $S_1$  and  $S_2$  as the count rates corresponding to the two polarizer positions. The pB counts are given by

$$\text{pB} = (S_1 - S_2)\delta t, \quad (1)$$

where  $\delta t$  is the exposure time (see Table 1 below). The statistical error of the pB is

$$\Delta \text{pB} = \sqrt{(S_1 + S_2)\delta t}. \quad (2)$$

Therefore, the S/N is given by:

$$\frac{\text{pB}}{\Delta \text{pB}} = \frac{(S_1 - S_2)\sqrt{\delta t}}{\sqrt{S_1 + S_2}} \quad (3)$$

Computing this S/N as a function of the exposure time in seconds for the typical number of counts at the observed height ( $1.9R_\odot$ ), we get  $\frac{\text{pB}}{\Delta \text{pB}} = 1.79\sqrt{\delta t}$ . Therefore, an exposure time on the order of 30 s is enough to achieve S/N=10. This S/N is high compared to the S/N that can be achieved observing the pB, with similar exposure at  $1.9R_\odot$ , using other presently available instruments. Although, the S/N of the pB measured with the WLC is high, we must bear in mind that our signal is the pB *fluctuations* - a fraction of the full pB. This reduces the actual S/N to about 3.

A possible source of instrumental error is the WLC mirror oscillations that may modulate the observed brightness, leading to false detection of pB fluctuations. The WLC exhibits fast exponential decay right after the end of the UVCS synoptic program (yet to be explained), with a settling time of about one hour and irregular low frequency fluctuations (timescale of the order of 0.5-1 hour). The second effect does not influence the pB fluctuation measurement since the frequencies that we measure are much higher. The exponential settling time has been taken into account in the few cases where it affects our data sets by removing those data points from our analysis.

In addition to white light data, we have also obtained Ly- $\alpha$  data with similar cadence and exposure time. We have investigated the variations in Ly- $\alpha$  intensity using similar methods as for the pB data. We found that the fluctuations in the Ly- $\alpha$  are within the magnitude expected from statistical fluctuations (i.e., S/N $\sim$ 1). This is due to the small number of photons reaching the detector, resulting in poor count statistics (order of 10 counts near the peak of the Ly- $\alpha$  emission line).

### 3. Observational Results

We have made several WLC observations in February 1997, February 1998, and February 1999 at  $1.9R_{\odot}$  in the south coronal hole, with exposures in the range of 30-100 seconds. The average pB count rate was approximately 300 counts per second. Table 1 lists the parameters of each observation: date, starting time and length, position angle (counterclockwise from the north pole), heliocentric height, cadence of pB measurements, exposure time, the frequency of the highest peak in the power spectrum, and the type of coronal structure (plume or interplume). For the February 1997 and 1998 observations the target – plume or interplume – was determined by measuring a spatial intensity profile in Ly- $\alpha$  at  $1.5R_{\odot}$  at the beginning of the observation and extrapolating the observed structure radially outward to  $1.9R_{\odot}$ .

#### 3.1. FFT analysis of pB at $1.9R_{\odot}$

In Figures 1-4 we show the observations of pB and the power spectra. The top panel shows the temporal evolution of the pB. The statistical relative error in the pB is on average 9.4%. The amplitude of the variations in pB is about three times the statistical error in the observations. We use the FFT spectral data analysis of the time-series (with the DC component and the small linear trend removed) to determine the frequency content of the fluctuations in pB.

The middle panel in Figures 1-4 shows the FFT power spectrum of the pB time sequence. The largest peak in Figure 1 appears at a frequency  $f = 1.6$  mHz with spectral resolution of 0.08 mHz. In Figure 2, the largest peak is at 1.7 mHz with spectral resolution of 0.03 mHz. In Figure 3, the largest peak is at 2.2 mHz. In Figure 4, the largest peak is at 0.5 mHz with the second largest peak at 1.2 mHz and with spectral resolution of 0.03

mHz. The peaks in the power spectrum of the pB indicate a periodicity consistent with the presence of compressional wave packets propagating in the coronal hole. The frequency of the peak power agrees with the expected range of frequencies for compressional waves driven by photospheric motions.

In order to investigate the statistical significance of the power spectrum we used the method developed by Welch (1967): the pB time sequence was divided into  $\sim 1$  hour segments. The segments were windowed using the Welch window, detrended, and Fourier transformed, and the spectra were averaged. The average spectrum of the one hour segments, with the appropriate statistical error, is shown in the bottom panel of Figures 1-4. The statistical errors were obtained by multiplying the average power spectrum by  $(1 \pm 1/\sqrt{N})$ , where  $N$  is the number of one hour segments (see Table 1). For example, for  $N = 9$  the standard deviation of the average spectrum is 33%. In Figure 1, it is evident that there is a peak in the power spectrum at 1.5 mHz, close to the frequency of the largest power in the power spectrum of the full observing sequence (middle panel). The spectral resolution of this power spectrum is about 0.3 mHz. The spectral resolution is reduced by the shorter duration of the data segments compared to the full data set. The close relation between the location of the highest peak in the full power spectrum and the averaged power spectrum is also evident in Figures 2-4. The length of each observing run determines the standard deviation of the average spectrum.

In Table 1, we show the frequency of the highest peak of the power spectrum that appears in the spectrum of each full time sequence, consistent with a peak in the average power spectrum of the segments at each observing run. Most of the observations exhibit the highest peak in the 1.6-1.8 mHz range. In the February 4, 1998 data, the highest peak occurred at 0.28 mHz with a smaller peak at 2.5 mHz. The peak at 2.5 mHz appears both in the raw power spectrum and in the averaged power spectrum, while the low frequency

power of the raw power spectrum appeared spread over 1 mHz in the averaged power spectrum. In the February 27, 1999 data, the highest peak occurs at 2.2 mHz, close to the range of frequencies in the February 1997 and 1998 observations. In the lower cadence February 28, 1999 data, the highest peak is near 0.5 mHz with the second highest peak at 1.4 mHz. The observations at two positions ( $1.9$  and  $2.1 R_{\odot}$ ) taken on February 5, 1998 and February 22, 1999 listed in Table 1 are described in detail in § 3.3 below.

A way to test whether the peaks in the power spectrum are due to aliasing is to obtain spectra with different cadences. The observations with cadence of 74.9 s (2/7/98; 2/6/98) and of 89.9 s (2/24/97; 2/3/98) show the largest peak at nearly the same frequency (1.6-1.8 mHz). The higher cadence (54 s) observations at 2/27/99 show a peak at 2.2mHz, and the lower cadence (123 s) observations on 2/28/99 show the second largest peak at 1.4 mHz. To further test for aliasing we have decreased the cadence by a factor of two by rebinning the data. The power spectrum of the rebinned data still shows the largest peaks at nearly the same frequencies, indicating that the peaks are not due to aliasing.

### 3.2. Wavelet analysis of pB at $1.9 R_{\odot}$

Since the wavelet transform was introduced in the early eighties (Grossmann & Morlet 1984), it has been widely used in signal and image processing. Like the FFT, the discrete wavelet transform (DWT) is a linear operation that defines a forward and inverse relationship between the time-domain and the frequency-domain (called the “wavelet domain”) with the appropriate basis functions. For the FFT, the basis functions are sine and cosine. For the DWT, the basis functions are more varied and complicated, and are usually called “wavelets.” Also, like the FFT, the DWT is orthogonal, making many operations computationally efficient. The advantage of the wavelet transform over the FFT is that the former allows the use of time-localized basis functions. This makes the

DWT better applicable for analysis of intermittent signals. In our case, the fluctuations in the pB appear as short duration (compared to the duration of the observation) pulses or wave-packets. Therefore, we use the *Morlet* wavelet (Grossmann & Morlet 1984) as our basis function, which is a sine wave with a Gaussian envelope

$$\psi(t) = \pi^{-1/4} e^{i\omega_0 t} e^{-t^2/2}, \quad (4)$$

where the parameter  $\omega_0 \approx 6$ .

For a given discrete time series  $T_{k'}$  such as our pB data, the DWT is

$$W_k(s) = \sum_{k'=0}^{K-1} T_{k'} \psi^* \left[ \frac{(k' - k)\delta t}{s} \right], \quad (5)$$

where  $s$  is the time scale (equivalent to wavelength in the FFT),  $k$  is the time index of the data points,  $K$  is the number of data points, and the asterisk denotes complex conjugate. The two-dimensional phase plots in Figures 5–8 below are constructed by plotting the wavelet amplitude for each inverse time scale  $1/s$  (i.e. “frequency”) as a function of time (i.e.  $k\delta t$ ) for the pB data shown in Figures 1–4.

In Figures 5–8, we show the wavelet phase diagram in which the horizontal axis is the time of observation, the vertical axis is the frequency in millihertz, and the colors correspond to the magnitude of the power at each frequency in arbitrary units. Examining the wavelet transforms of the pB time series it becomes evident that the quasi-periodic density fluctuations appear intermittently during the observations with a coherence time of about 30 minutes. The line plot on the left panel in Figures 5–8 represents a the time-averaged wavelet spectrum. The good agreement between the average wavelet spectrum and the FFT power spectrum at the bottom panel in Figures 1–4 is encouraging and provides additional credibility to the spectral structure of the pB signal.

### 3.3. Cross-correlation analysis at $1.9R_{\odot}$ and $2.1R_{\odot}$

In order to establish the wave origin of these fluctuations with higher confidence we have attempted to determine their group speed by observing the pB at two separate radially aligned points at  $1.9R_{\odot}$  and at  $2.1R_{\odot}$ . The observations were taken on February 5, 1998 at 14:46UT with a cadence of 89.5 s and an exposure of 60s for  $\sim 9$  hours and on February 22, 1999 at 16:56UT (Fig. 9) with a cadence of 74 s and an exposure of 45 s for  $\sim 8$  hours with about 4 hours of a continuous sequence (see Table 1). The WLC pointing was alternated between the two locations once every 3 pB measurements. The white light brightness at  $1.9R_{\odot}$  and  $2.1R_{\odot}$  are shown at the top panel of Figure 9. As expected, the white light brightness of the corona is lower at  $2.1R_{\odot}$  than at  $1.9R_{\odot}$ . The pB at  $1.9R_{\odot}$  (triangles) and at  $2.1R_{\odot}$  (stars) are shown in the middle panel.

Since we expect the highest correlation between the two quasi-periodic signals when the fluctuations at  $1.9R_{\odot}$  reach  $2.1R_{\odot}$ , we look for peaks of the cross-correlation function. The peaks in the correlation will occur when a wave packet detected at  $1.9R_{\odot}$  will reach  $2.1R_{\odot}$ . For a truly periodic wave the peaks in the cross-correlation function occur when the two pB signals are in phase (i.e., shifted by a full wavelength). Negative correlation will occur when the waves are out of phase. A high correlation at a negative time lag may also occur for periodic propagating waves.

The cross-correlation of the pB at  $1.9R_{\odot}$  and  $2.1R_{\odot}$  is shown in the bottom panel of Figure 9. In order to determine how significant the cross-correlation is - we show the level of cross-correlation (dashed lines) that would have been produced by two white-noise signals. Approximately 95% of the noise cross-correlation should lie between these bounds given by  $\pm 1.96/\sqrt{n}$ , where  $n$  is the number of data pairs (Brockwell & Davis 1987). No significant correlation was found in the February 5, 1998 data set. However, the February 22, 1999 data (Figure 9) show that the cross-correlation at time lag of  $656 \pm 165$  s is significantly above

the noise level and may have been caused by a propagating wave packet between the two points. The time lag error is  $\pm$  half the time between adjacent time lags. By dividing the distance between the two points ( $0.2R_{\odot}$ ) by the time lag of the peak correlation we obtain the propagation speed of the fluctuation,  $\sim 210 \pm 54 \text{ km s}^{-1}$ , assuming radial propagation.

The deduced propagation speed corresponds to the group speed of the compressional wave plus the background solar wind speed at about  $2R_{\odot}$ . If we take  $150 \pm 60 \text{ km s}^{-1}$  for the solar wind speed at  $2R_{\odot}$  based on UVCS Doppler dimming observations in coronal holes (Cranmer et al. 1999) we get  $\sim 60 \pm 81 \text{ km s}^{-1}$  for the wave speed. The large uncertainty in the wave speed does not allow the determination of whether we have detected a propagating wave.

The uncertainty may be reduced if we use the solar wind speed based on mass flux conservation at  $2R_{\odot}$ , which is  $90 \pm 20 \text{ km s}^{-1}$  (Cranmer et al. 1999). In this case, we get the wave speed of  $120 \pm 58 \text{ km s}^{-1}$  in agreement with the expected sound speed in  $10^6 \text{ K}$  plasma. In the linear approximation (i.e., for small wave amplitudes) the waves can be viewed as perturbations propagating on top of a background time-averaged, solar wind flow, where the time averaging is at the wave period. The mass flux conservation represents the solution of the equation of continuity for the background flow, on times scales larger than the wave periods (i.e., with the waves averaged out). We use the approximation that on long time scales the mass flux is conserved in order to estimate the background solar wind flow.

In order to improve the determination of the wave speed we need to reduce the possible noise level by increasing the number of data pairs. In addition, we found from the wavelet analysis of the fluctuations that the coherence length is of the order of 30 min. Therefore, we need higher cadence observations at the two radial distances to determine the wave speed with higher statistical confidence.

#### 4. Conclusions

Observations with the UVCS WLC channel of pB fluctuations indicate that the density in the south polar coronal hole at  $1.9R_{\odot}$  fluctuates on a time scale of about 1.2-2.5 mHz, with possibly lower and higher frequencies in the millihertz range. This is the first detailed high-cadence observation of such fluctuations at a considerable distance above the solar limb. The temporal evolution and the spectrum suggest that these fluctuations may be generated by compressional waves propagating from the Sun. The fact that the density fluctuations spectrum is peaked in a narrow frequency band at the expected range of frequencies strongly suggest the likelihood of wave related phenomena. Our observations are consistent with the recently reported (DeForest and Gurman 1998) detection of compressional waves by EIT in polar plumes closer to the limb ( $< 1.2R_{\odot}$ ). These waves were identified as slow magnetosonic waves by Ofman, Nakariakov, & DeForest (1999).

The fluctuations may be generated by the nonlinear compressive waves driven locally by nonlinear Alfvén waves (Ofman & Davila 1997a, 1997b, 1998). The nonlinear Alfvén waves provide an additional source of energy for the acceleration of the fast solar wind. The spatial and temporal variations of the Alfvén wave amplitude in coronal holes generates variations in the wave pressure that drives the compressional nonlinear waves. However, further studies are needed to relate quantitatively the results of present observations to these waves. For example, the difference between the nonlinear compressional waves speed and the linear slow magnetosonic waves speed is too small to distinguish with the present accuracy of measurement.

These waves could also be driven by density fluctuations at the base of the coronal hole, driven by the solar p-mode oscillations that propagate into the corona in the form of fast or slow magnetosonic waves. Since the peak power of the photospheric motions occurs at 3.3 mHz this suggests that the p-mode energy may contribute to the observed waves at about

half the above frequency due to nonlinear period doubling that occurs in the transition region. However, it is not obvious how the p-mode fluctuation could transfer their energy to the slow and fast mode in the corona, and we do not attempt to solve this problem in the present paper. Since the energy flux in slow waves is only a small fraction of the energy contained in p-mode oscillations - even small conversion efficiency could potentially account for the observed waves. It is possible that other mechanism (such as reconnection in the magnetic network at the base of the corona) may generate the observed waves.

The temporal evolution of the frequency spectrum of the pB as seen in the wavelet analysis indicates that the waves are produced in short bursts of about 30 minutes throughout the observation. The waves appear intermittently both in plume and in interplume regions. However, due to line-of sight effects, contributions from both regions are most probably contained in any single observation.

The measurement of the propagation speed of the fluctuations produced velocities in the range of 150-260 km s<sup>-1</sup> at  $2R_{\odot}$ . This range of speed is consistent with the phase speed of slow magnetosonic waves or nonlinear solitary-like waves carried by the solar wind in the low- $\beta$  coronal hole plasma and is an encouraging result. The nonlinear solitary-like wave speed is about 20%-30% faster than the sound speed for typical coronal hole parameters (Ofman & Davila 1997a). Linear slow magnetosonic waves propagate at a speed close to the sound speed in the low- $\beta$  coronal hole plasma. Measurements of the solar wind speed and of the ambient temperature (in order to determine the sound speed) close to the sun with an accuracy of 10% or better are needed in order to distinguish between the above wave modes.

The likely detection of compressional waves in the south polar coronal hole far above the limb may be the source of the additional momentum and heat required to accelerate the fast solar wind in coronal holes. The slow waves are damped by compressive viscosity

close to the Sun and by Landau damping in collisionless plasma. Preliminary calculation of compressive dissipation of slow magnetosonic waves shows that the low-frequency slow waves should still be apparent at  $1.9R_{\odot}$  for the theoretically predicted solar value of the compressive viscosity. It is evident that additional observations and models are needed in order to establish the role of these waves in the heating and the acceleration of the solar wind.

This work is supported by the National Aeronautics and Space Administration under grant NAG5-3192 to the Smithsonian Astrophysical Observatory, by Agenzia Spaziale Italiana, by Swiss funding through ESA's PRODEX programs, national funds and the Swiss Federal Institute of Technology Zurich, and by NASA SOHO Guest Investigator Program (NASW-98024). LO would like to thank Dr. J.M. Davila for helpful discussions. We would also like to thank Dr. Frederic Baudin for providing us with his wavelet transform routines, and Ms. Neelima Sehgal for proofreading the manuscript.

## REFERENCES

- Brockwell, P.J., & Davis, R.A. 1987, *Time Series: Theory and Methods*, Springer-Verlag, New York
- Cranmer, S.R., et al. 1999, ApJ, 511, 481
- DeForest C.E., et al. 1997, Sol. Phys., 175, 393.
- DeForest, C.E., and J.B. Gurman 1998, ApJ, 501, L217.
- Delaboudinière J.-P., et al. 1995, Sol. Phys., 162, 291.
- Fisher, R.R. & Guhathakurta, M. 1995, ApJ, 447, L139.
- Grossmann, A., & Morlet, J. 1984, SIAM J. Math. Anal., 15, 723
- Holzer, T.E., & Leer, E. 1980, J. Geophys. Res., 85, 4665
- Kohl, J.L. et al. 1995, Solar Physics, 162, 313
- Ofman, L., & Davila, J.M. 1995, J. Geophys. Res., 100, 23413.
- Ofman, L., Davila, J.M. 1997a, ApJ, 476, 357
- Ofman, L., Davila, J.M. 1997b, ApJ, 476, L51
- Ofman, L., Davila, J.M. 1998, JGR, 103, 23677
- Ofman, L., Nakariakov, V., & DeForest, C.E.: 1999, ApJ, 514, 441
- Ofman, L., Romoli, M., Poletto, G., Noci G., Kohl, J.L., 1997, ApJ, 491, L111
- Ofman, L., Romoli, M., Poletto, G., Noci G., Kohl, J.L., 1998, ApJ, 507, L189
- Phillips, J.L. et al. 1995, Geophys. Res. Lett., 22, 3301

Romoli, M., Benna, C., Cranmer, S., Fineschi, S., Gardner, L.D., Strachan, L., Kohl, J.L.,  
Noci, G., 1997, 5th SOHO Workshop, ESA SP-404, pp. 633-636

Welch, P.D. 1967, IEEE transactions, 15, 2

Wagner, W.J. 1976, ApJ, 206, 583

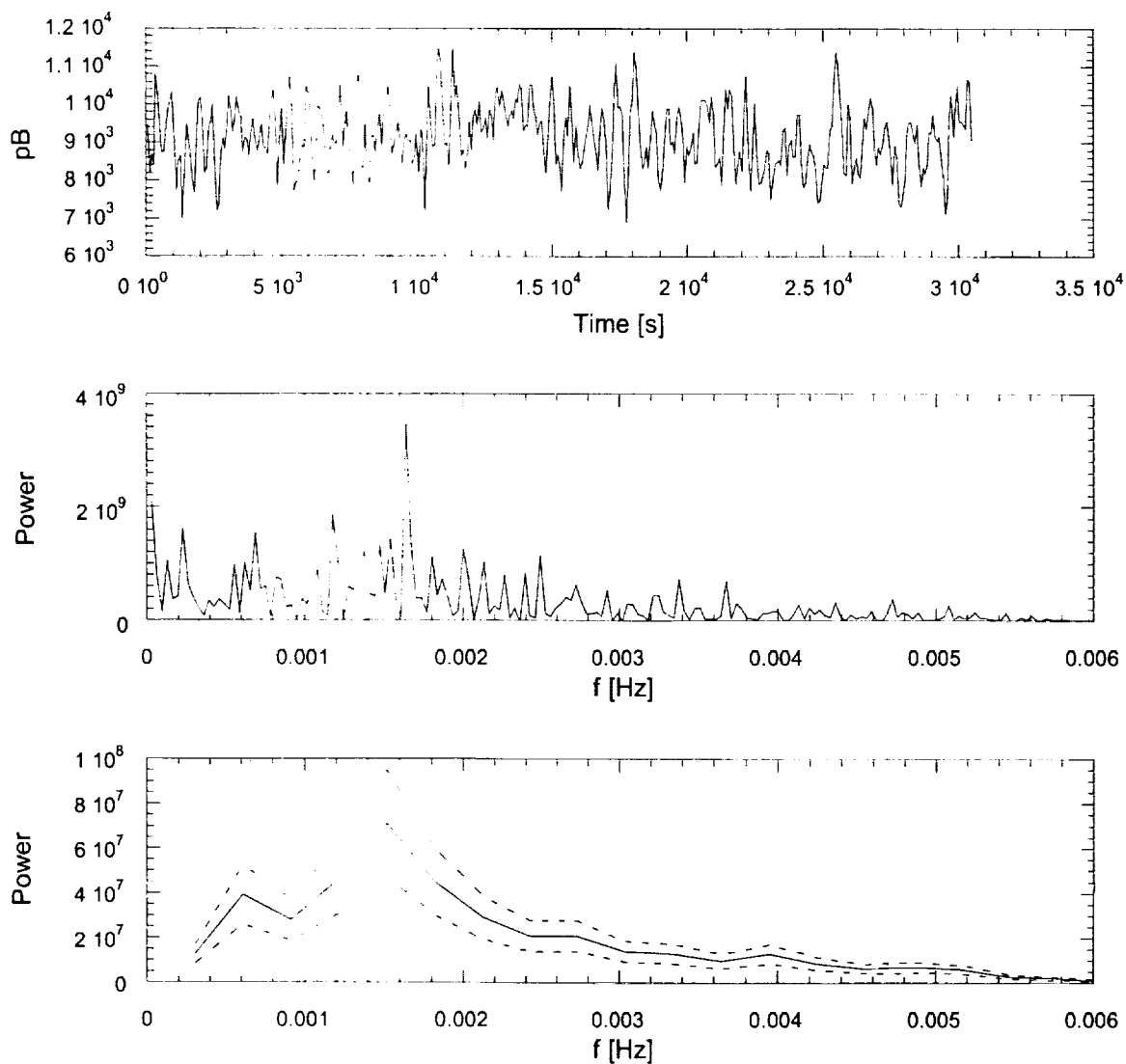


Fig. 1.— Time variation of the polarized brightness observed with the UVCS WLC in the south polar coronal hole at  $1.9R_{\odot}$  on February 6, 1998 with 45 s exposure (top panel). The polarized brightness units are given relative to the Sun center brightness integrated over the WLC wavelength bandpass (450-600 nm). The power spectrum of the pB (middle panel) and averaged power spectrum of nine  $\sim 1$  hour segments showing the  $\pm$  standard error interval (lower panel).

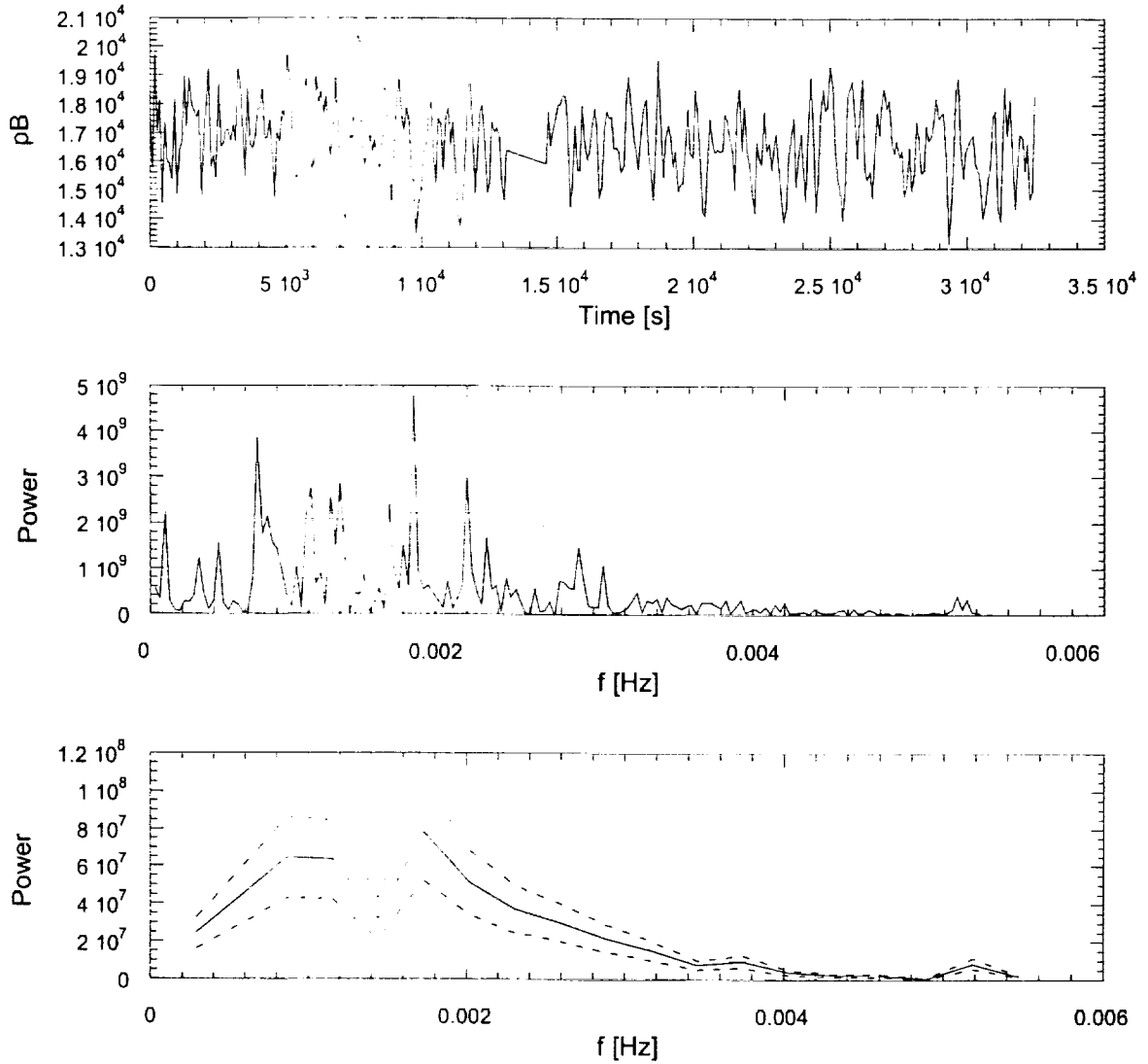


Fig. 2.— Same as Figure 1 for observations taken on February 3, 1998 with 60 s exposure (top panel). Initial settling time of the mirror was removed from the analysis. The power spectrum of the pB (middle panel) and averaged power spectrum of nine  $\sim 1$  hour segments showing the  $\pm$  standard error interval (lower panel).

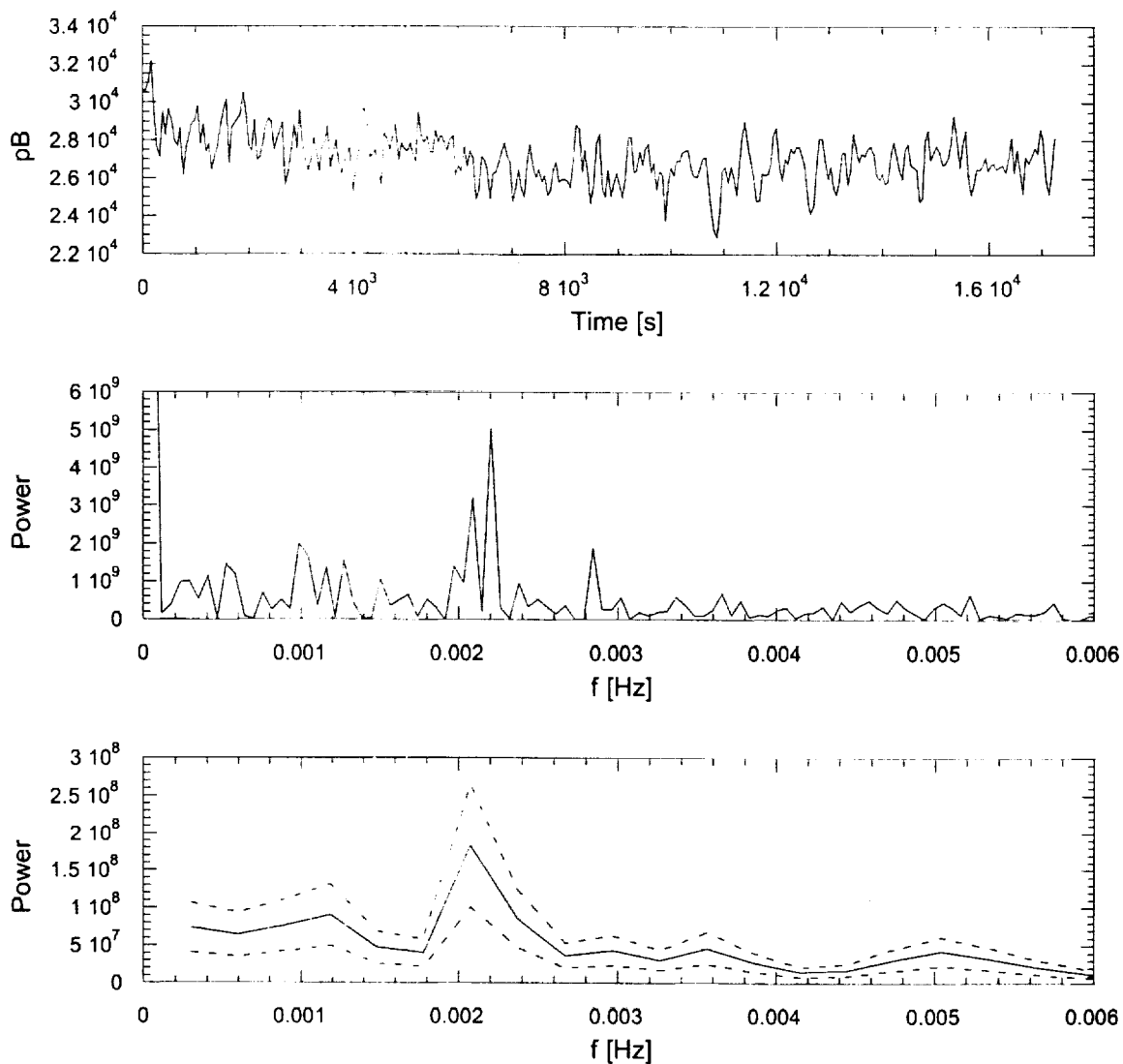


Fig. 3.— Same as Figure 1 for observations taken on February 27, 1999 with 30 s exposure (top panel). The power spectrum of the pB (middle panel) and averaged power spectrum of five  $\sim 1$  hour segments showing the  $\pm$  standard error interval (lower panel).

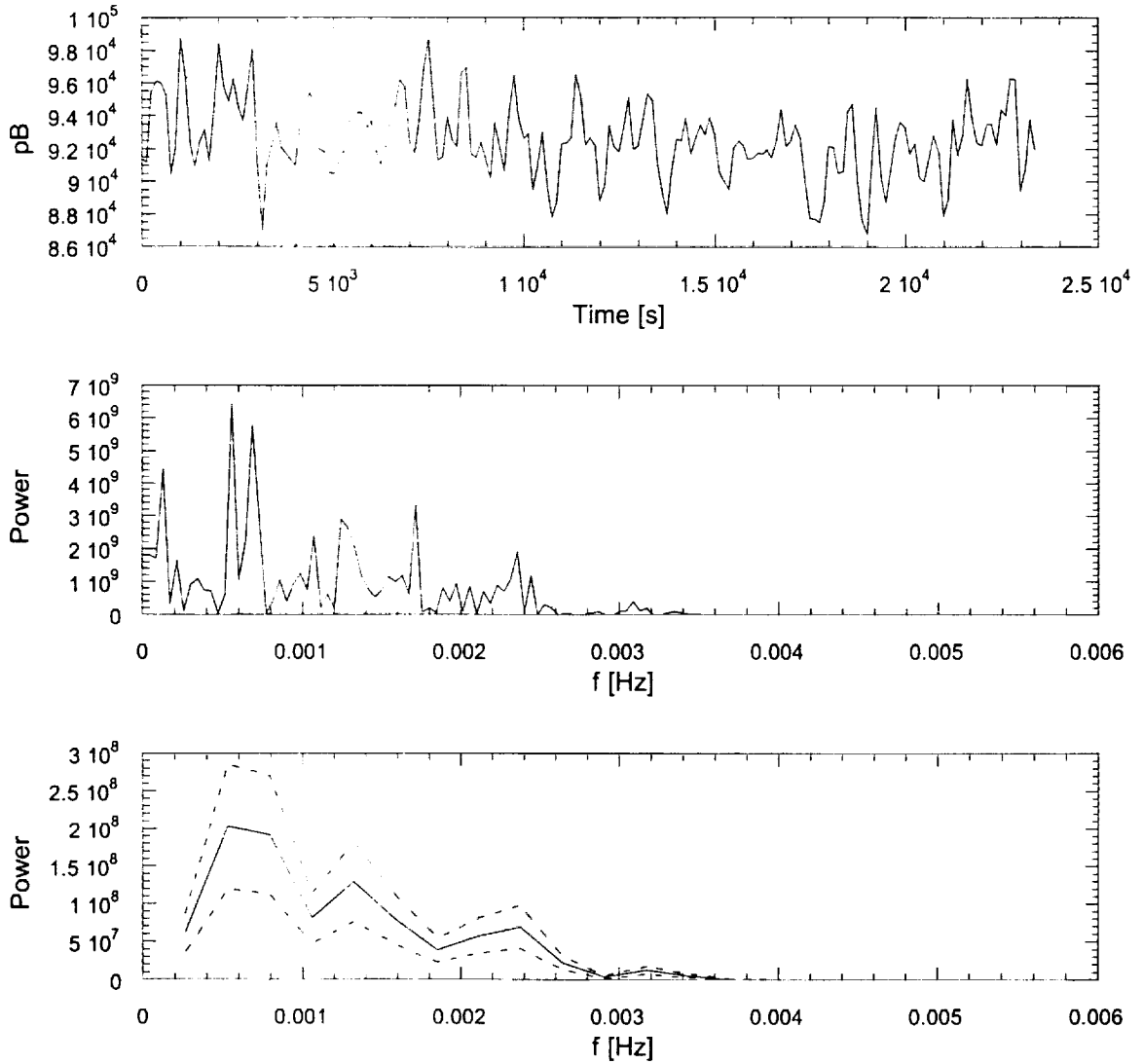


Fig. 4.— Same as Figure 1 for observations taken on February 28, 1999 with 100 s exposure (top panel). The power spectrum of the pB (middle panel) and averaged power spectrum of six  $\sim$  1 hour segments showing the  $\pm$  standard error interval (lower panel).

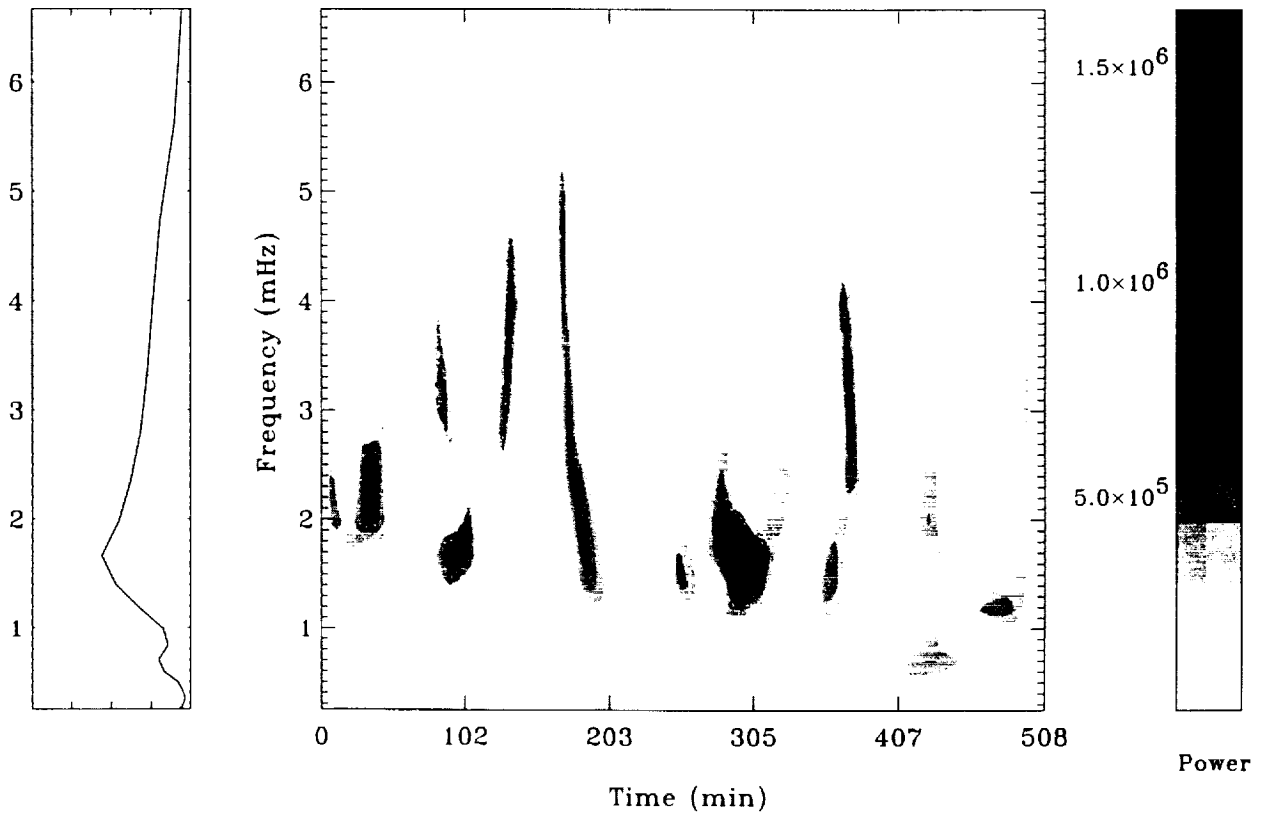


Fig. 5.— Wavelet analysis of the pB data taken on February 6, 1998. The strongest fluctuations appear in  $\sim 30$  minute bursts. The time-averaged spectrum is similar to the averaged FFT power spectrum in Figure 1.

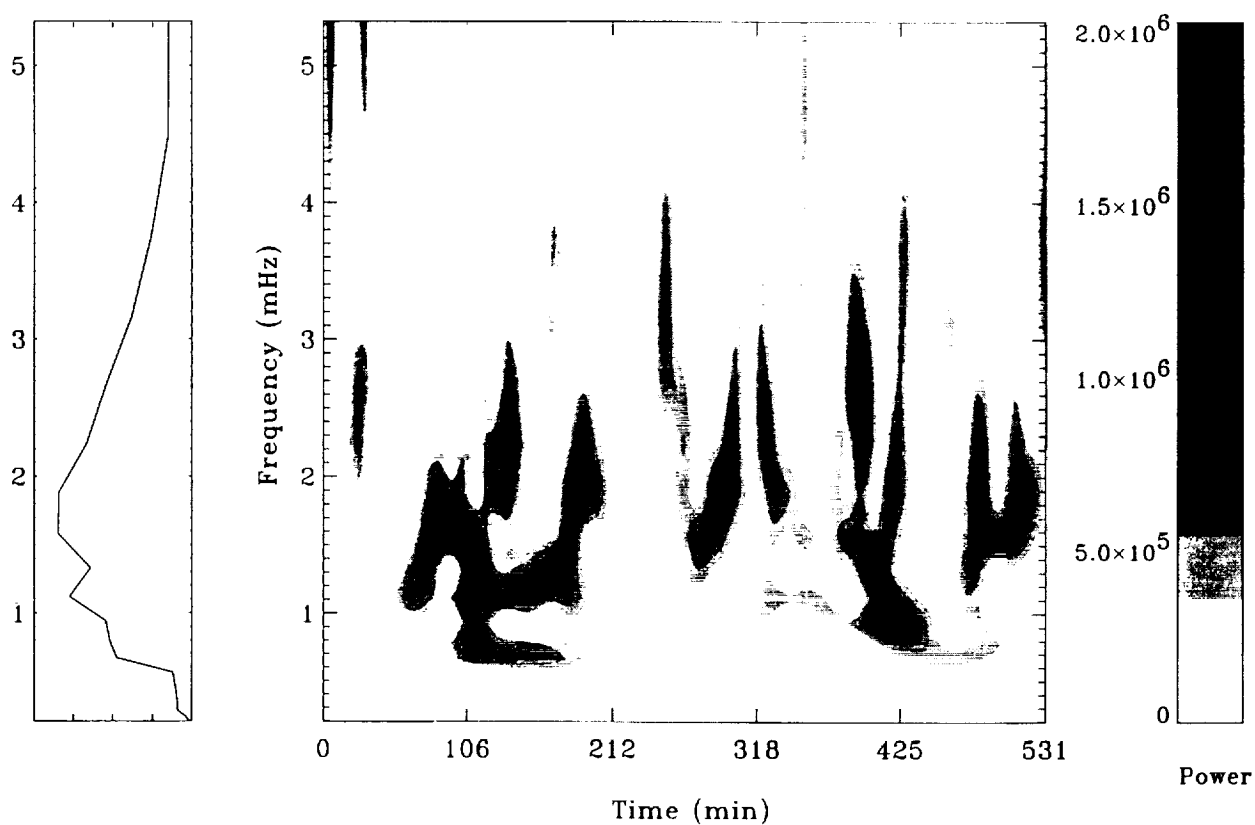


Fig. 6.— Wavelet analysis of the pB data taken on February 3, 1998. The strongest fluctuations appear in short bursts in the 1-3 mHz range. The time-averaged spectrum is qualitatively similar to the averaged FFT power spectrum in Figure 2.

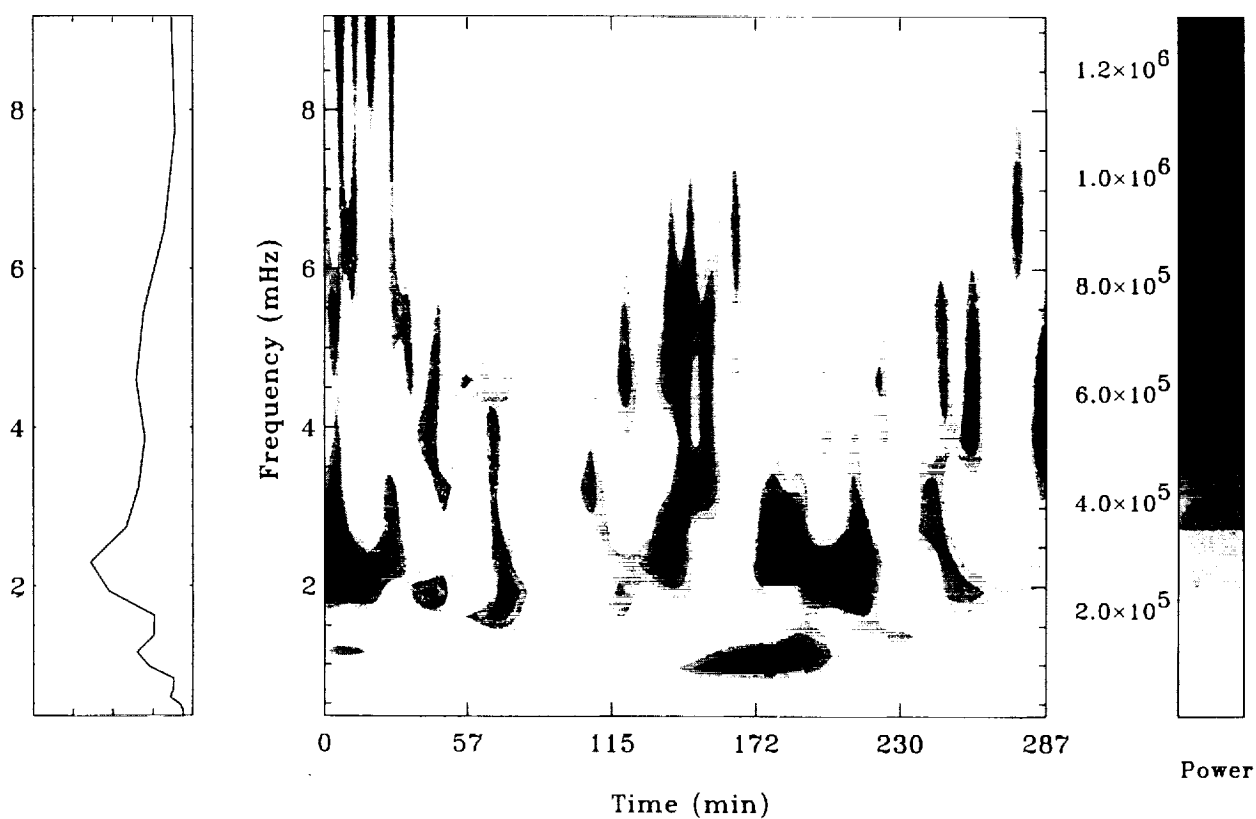


Fig. 7.— Wavelet analysis of the pB data taken on February 2, 1999. Note that the strongest fluctuations appear in short bursts. The time-averaged spectrum is qualitatively similar to the averaged FFT power spectrum in Figure 3.

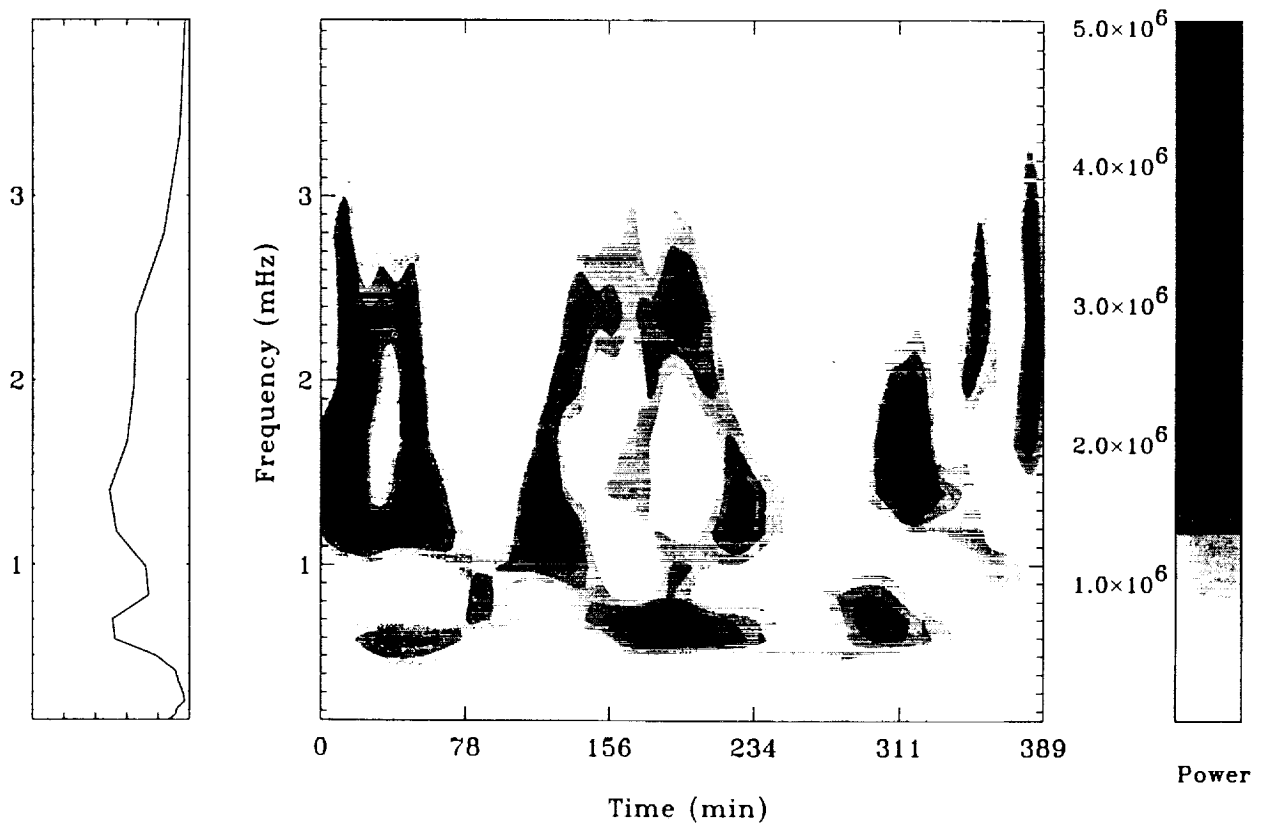


Fig. 8.— Wavelet analysis of the pB data taken on February 28, 1999. Note that the strongest fluctuations appear in short bursts. The time-averaged spectrum is qualitatively similar to the averaged FFT power spectrum in Figure 4.

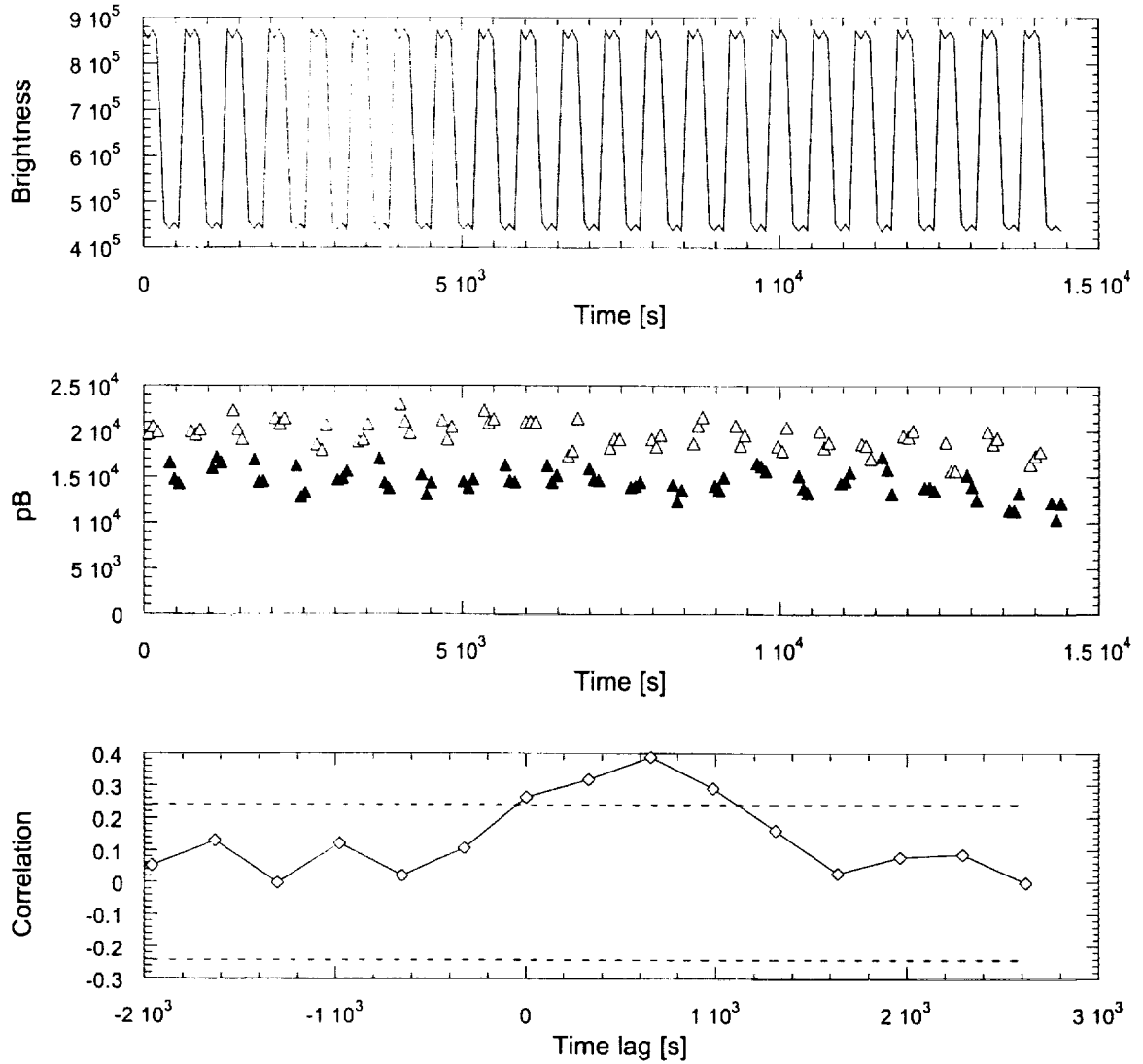


Fig. 9.— The WLC observations of white light brightness at  $1.9R_{\odot}$  and  $2.1R_{\odot}$  (top panel). The pB at  $1.9R_{\odot}$  (triangles) and at  $2.1R_{\odot}$  (stars) are shown in the middle panel. The cross-correlation of the pB at  $1.9R_{\odot}$  and  $2.1R_{\odot}$  (bottom panel). The cross-correlation expected from white noise is marked by the dashed lines.

Table 1: The parameters of the high cadence UVCS WLC observations of pB fluctuations

Date	Start (UT)	Duration (h)	Position Angle	Distance ( $R_{\odot}$ )	Cadence (s)	Exposure (s)	Peak power $f$ (mHz)	Location
24 Feb 1997	21:27	3.7	184.1°	1.9	89.9	60	1.8	Plume
3 Feb 1998	14:19	9.9 <sup>a</sup>	180.0°	1.9	89.9	60	1.7	Plume
4 Feb 1998	14:30	10.0	180.0°	1.9	89.9	60	2.5	Interplume
5 Feb 1998	14:47	9.1	180.0°	1.9 & 2.1	89.5 <sup>b</sup>	60	N/A	Interplume (?)
6 Feb 1998	15:55	8.5	173.3°	1.9	74.9	45	1.6	Interplume
7 Feb 1998	15:19	9.1	175.7°	1.9	74.9	45	1.7	Plume
22 Feb 1999	16:56	4.0 <sup>c</sup>	179.6°	1.9 & 2.1	74.7 <sup>b</sup>	45	N/A	N/A
27 Feb 1999	16:08	4.8	180.0°	1.9	54.2	30	2.2	N/A
28 Feb 1999	11:13	6.6 <sup>c</sup>	180.0°	1.9	122.8	100	0.5	N/A

<sup>a</sup> The pB were interpolated in the 0.40 h data gap after 4.5 h of observations.

<sup>b</sup> It takes additional  $\sim 32$  s to move the mirror between the two positions.

<sup>c</sup> Uninterrupted observing time.